VTT Technical Research Centre of Finland

Mechanical and optical properties of as-grown and thermally annealed titanium dioxide from titanium tetrachloride and water by atomic layer deposition

Ylivaara, Oili M.E.; Langner, Andreas; Liu, Xuwen; Schneider, Dieter; Julin, Jaakko; Arstila, Kai; Sintonen, Sakari; Ali, Saima; Lipsanen, Harri; Sajavaara, Timo; Hannula, Simo-pekka; Puurunen, Riikka L.

Published in:
Thin Solid Films

DOI:
10.1016/j.tsf.2021.138758

Published: 31/08/2021

Document Version
Publisher's final version

Thin Solid Films 732 (2021) 138758

Contents lists available at ScienceDirect

Thin Solid Films

journal homepage: www.elsevier.com/locate/tsf

Mechanical and optical properties of as-grown and thermally annealed titanium dioxide from titanium tetrachloride and water by atomic layer deposition

Oili M.E. Ylivaara [a,*], Andreas Langner [a], Xuwen Liu [b], Dieter Schneider [c], Jaakko Julin [d], Kai Arstila [d], Sakari Sintonen [e], Saima Ali [e], Harri Lipsanen [e], Timo Sajavaara [d], Simo-Pekka Hannula [b], Riikka L. Puurunen [a,b]

[a] VTT Technical Research Centre of Finland, P. O. Box 1000, FI-02044 VTT, Finland
[b] Aalto University, School of Chemical Engineering, Department of Chemical and Metallurgical Engineering, P.O. Box 16100, FI-00076 AALTO, Finland
[c] Fraunhofer IWS Dresden, Winterbergstrasse 28, Dresden 01277, Germany
[d] University of Jyväskylä, Department of Physics, P. O. Box 35, Jyväskylä FI-40014, Finland
[e] Aalto University School of Electrical Engineering, Department of Electronics and Nanoengineering, P. O. Box 13500, Aalto FI-00076, Finland

ARTICLE INFO

Keywords:
ALD
Atomic Layer Deposition
TiO_2
residual stress
optical properties
elastic modulus
hardness

ABSTRACT

The use of thin-films made by atomic layer deposition (ALD) is increasing in the field of optical sensing. ALD TiO_2 has been widely characterized for its physical and optical properties, but systematic information about the influence of thermal history to optical and mechanical properties of the film is lacking. Optical applications require planar surface and tunability of the refractive index and residual stress. In addition, mechanical properties such as elastic modulus and film hardness influence the performance of the layer, especially, when optics is integrated with microelectromechanical systems. In this work, optical properties, density, elemental analysis, residual stress, elastic modulus and hardness of as-grown ALD TiO_2 thin films on silicon were studied at temperature range from 80 to 350 °C and influence of post-ALD thermal annealing was studied on films annealed up to 900 °C. ALD TiO_2 films were under tensile stress in the scale of hundreds of MPa. The stress depended both on the ALD temperature and film thickness in a complex way, and onset of crystallization increased the residual stress. Films grown at 110 and 300 °C were able to withstand post-ALD annealing at 420 °C without major change in residual stress, refractive index or extinction coefficient. Elastic modulus and hardness increased upon crystallization with increasing ALD temperature. The results presented here help to improve the design of the optical devices by choosing films with desired optical properties, and further help to design the post-ALD thermal budget so that films maintain their desired features.

1. Introduction

TiO_2 is a polymorphic material [1,2], and at temperature range used in thermal atomic layer deposition (ALD), it exists at least in amorphous, anatase and rutile forms [3–6]. Its electrical [7–9] and optical properties [10–14] depend on the film morphology. Titanium dioxide (TiO_2) grown by ALD from titanium tetrachloride ($TiCl_4$) and deionized water (H_2O) has been widely studied since the first experiments under the names of molecular layering and atomic layer epitaxy [15–18]. The nucleation and the growth of ALD TiO_2 is known to be sensitive to different substrates and substrate terminations [4,19–31]. The onset of crystallisation and the grain growth are shown to be both thickness, and growth temperature dependent [19,21,32–42].

Considering the use of ALD TiO_2 in optical applications requires precise understanding, not only of the desired optical properties of the grown films, but also of the material properties and their dependence on process conditions. For ALD TiO_2, both tensile and compressive residual stress have been measured at temperature range from 80 to 300 °C depending on the used substrate material [13,43,44,48]. The mechanical properties such as elastic modulus and hardness, have been studied by X-ray methods [45,46], interfacial mechanical testing [47] and nanoindentation [48–50]. As post-ALD thermal treatments are known to create, for example adhesion problems [51], it is important to do systematical characterization of the relation of processing conditions to

* Corresponding author.

https://doi.org/10.1016/j.tsf.2021.138758
Received 2 October 2020; Received in revised form 5 March 2021; Accepted 20 May 2021
Available online 26 May 2021

optical and mechanical properties of the material.

The goal of this work was to gain better understanding of the residual stress, elastic modulus, and hardness in ALD TiO_2 films related to their use in optical applications. The physicochemical, mechanical, and system properties of ALD TiO_2 were studied as a function of process temperature, film thickness and storage time in air. Investigations on the effect of the post-ALD annealing on optical properties and residual stress of the TiO_2 film were also carried out. This article continues the article series on mechanical characterization of ALD thin films previously published on Al_2O_3 [49,52,53], Al_2O_3-TiO_2 nanolaminates[49,54,55,56] and TiO_2[48,49,53].

2. Experimental

2.1. Sample preparation

ALD TiO_2 films were grown on 150 mm p-type (100) silicon wafers from Okmetic Oyj. Double side polished (DSP) 380 ± 5 μm thick wafers were used for the wafer curvature measurements, and single side polished (SSP) wafers of 675 ± 15 μm for other characterization. Wafers were wet cleaned before ALD using RCA -cleaning (SC-1, DHF and SC-2). Cleaned wafers were covered with 1 - 2 nm thick chemical oxide. The major reason for the use of the RCA -cleaned silicon surface was to get controllable surface condition for the film growth.

The ALD reactor was a single-wafer Picosun® R-150 tool with three reactant lines. The tool was equipped with a load-lock. The intermediate space pressure was about 7 hPa. There was a constant 200 sccm ultrapure nitrogen 6.0 flow through the reactant lines to the reaction space, and 300 sccm nitrogen flow to the intermediate space located between the reaction space and the heated vacuum chamber wall. Electronic grade $TiCl_4$ from SAFC Hitech with purity of 99.995%, and deionized H_2O with resistivity of 18.2 MΩ·cm were used as precursors. The $TiCl_4$ bubbler was kept at 14 °C with a Peltier cooling element, and the bubbler for the H_2O at room temperature. $TiCl_4$ and H_2O precursor dose and purge times were 0.1 and 4.0 s, respectively. The growth temperature was varied from 80 to 350 °C, and the number of growth cycles from 190 to 7400, corresponding nominal film thicknesses of about 10 to 300 nm. As the pulse and purge times were kept constant through the temperature range, we are aware that the process may not have fully corresponded to saturated ALD, especially at lower growth temperatures.

The influence of the post-ALD annealing on optical properties and residual stress was studied on low resistivity, 380 ± 5 μm thick, DSP silicon wafers to enable reliable optical measurements also in the near infrared (NIR) region. Films were grown at temperature range from 110 to 300 °C, and selected samples were post-ALD annealed at 300, 450, and 900 °C for 30 min under 1000 sccm nitrogen flow. The annealing furnace was ATV Technologies GmbH PEO-603. Films examined were targeted to be 100 nm thick.

2.2. Characterization

Film thicknesses were measured with spectroscopic reflectometry SCI FilmTek 2000M, and 49-point automated measurement recipe. The refractive index and extinction coefficient for the automated measurement recipe were determined, from films grown at 300 °C (using 5000 cycles), with SCI FilmTek 4000 at wavelength range from 480 to 1650 nm. For some wafers, thickness and refractive index were measured with a Plasmos spectroscopic ellipsometry using 633 nm wavelength (HeNe -laser) and 70° incident angle. Optical characterization of refractive index and extinction coefficient over a range from UV to NIR on wavelength range from 190 to 1650 nm was done using spectroscopic reflectometry SCI FilmTek4000. Optical measurements were done after ALD, and repeated after post-ALD thermal annealing at 300, 450 and 900 °C.

X-ray reflectivity (XRR) and a gracing incidence X-ray diffraction (GIXRD) analysis were carried out using a Philips X'Pert Pro diffractometer. Film thickness, density and crystallographic structure were measured and analyzed using Cu-alpha wavelength with 40 kV / 40 mA voltage and current, respectively. Crystallite sizes were calculated using Scherrer equation [57] from (101) peak. Selected samples were also examined for crystallinity with tapping mode atomic force microscopy (AFM), Digital Instruments NanoScope Dimension 3100 equipment using 3 x 3 μm scan and 512 sample size. AFM rms roughness was analyzed for samples after first order flattening.

Time-of-flight elastic recoil detection analysis (TOF-ERDA) was made with self-built equipment using 10.2 MeV ^{35}Cl and 11.9 MeV ^{63}Cu ions from a 1.7 MV Pelletron accelerator [58]. Rutherford backscattering (RBS) was used to determine the Cl levels.

Residual stress was determined by the wafer curvature method using Veeco DEKTAK V200-Si stylus profilometer. Wafer curvature was measured before and after ALD using 120 mm long scan parallel and perpendicular to the wafer flat, and residual stress was calculated using Stoney's equation [59,60]. For selected wafers, the residual stress was determined after ALD, and after post-ALD annealing using laser-based wafer curvature measurement tool, Toho Technology FLX-2320-S equipment, and 120 mm scan in parallel and perpendicular to the wafer flat. In both cases the residual stress values were reported with the maximum measurement uncertainty as calculated in Ref. [52]. The maximum measurement uncertainty for these two tools are different mostly, because of the uncertainty in the bow measurement and wafer placement. For example, in the case of ALD Al_2O_3 under 200 MPa residual stress, the maximum measurement uncertainty composes of three

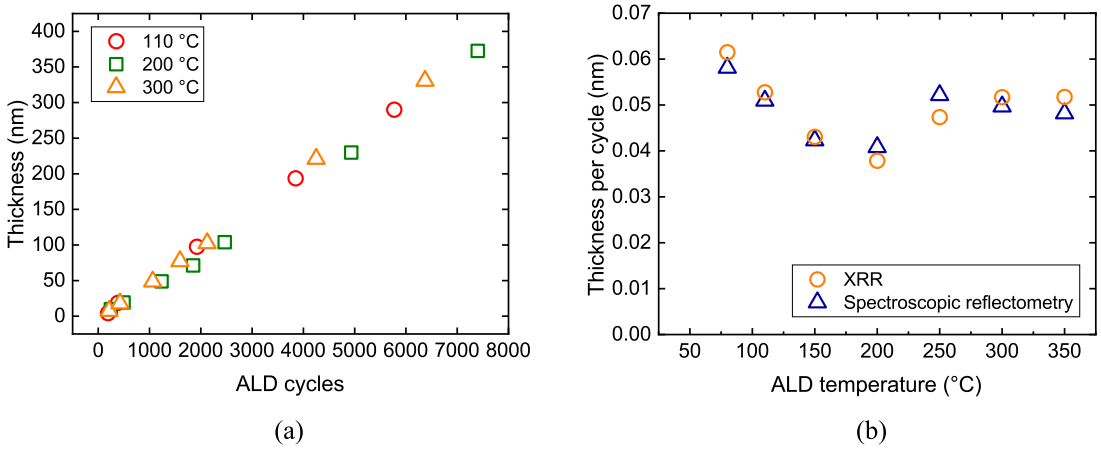

Fig. 1. (a) Thickness as a function of ALD cycles for TiO_2 grown at 110, 200 and 300 °C on silicon. In (b) average growth per cycle is presented as a function of ALD temperature. GPC values, calculated from thickness values measured with XRR and spectroscopic reflectometry were in line.

Table 1
Spectroscopic reflectometry, ellipsometry, XRR and XRD results measured for ALD TiO_2 thin films. The growth per cycle values was calculated from thickness measured by reflectometry divided by the number of growth cycles.

Growth temperature [°C]	Growth cycles	Reflectometer thickness (49 pts) [nm]	St.dev.(49 pts) [nm]	St.dev. (49 pts) [%]	Thickness/ cycles [nm]	Refractive index @633 nm (5 pts)	XRR thickness [nm]	XRR density [g/cm3]	XRR roughness [nm]	GIXRD observed peaks	Crystallite size from (101) peak [nm]
80	1662	96.6	1.9	2.0	0.0581	-	102.2	3.55	0.5	-	-
110	1924	98.0	2.2	2.2	0.0510	2.42	101.5	3.70	0.2	-	-
150	2312	97.8	2.6	2.7	0.0423	2.45	99.5	3.75	0.3	-	-
200	247	9.8	0.3	3.0	0.0401	-	9.5	3.75	0.4	-	-
200	493	18.6	0.5	2.7	0.0377	-	18.0	3.75	0.4	-	-
200	1233	48.8	1.2	2.4	0.0497	-	47.7	3.85	0.4	(101)	32.3
200	1850	71.3	2.3	3.2	0.0385	-	67.0	3.90	0.7	(101), (004), (200), (211), (204)	26.6
200[1]	2467	100.7	2.9	2.9	0.0408	2.60	93.4	3.85	0.8	(101), (103), (004), (112), (200), (105), (211), (204), (215)	29.7
200[1]	2467	103.9	3.8	3.7	0.0421	2.66	92.9	3.85	1.2	(101), (004), (200), (105) (211), (204)	27.6
200[2]	4933	229.8	7.1	3.1	0.0466	-	-	-	-	(101), (103), (004), (112), (200), (105), (211), (204)	28.9
200[2]	7400	372.6	8.0	2.1	0.0504	-	-	-	-	(101), (103), (004), (112), (200), (105), (211), (204), (215)	32.1
250	1953	101.9	0.6	0.6	0.0522	2.59	92.4	3.70	3.2	(101), (112), (200), (211), (204),(202)	26.9
300	319	13.0	0.6	4.6	0.0408	-	11.9	3.80	1.0	(101)	14.3
300	531	23.2	0.3	1.3	0.0437	-	21.2	3.80	1.6	(101), (211)	27.0
300	1062	48.3	0.6	1.2	0.0455	-	45.5	3.80	3.3	(101), (200)	24.2
300[3]	2124	105.5	0.8	0.8	0.0497	2.73	109.8	3.85	3.3	(101), (004), (200), (105), (211), (204),(202)	24.0
300[3]	2124	101.5	1.0	1.0	0.0478	-	91.5	3.80	4.3	(101), (200), (211)	23.0
300[2]	6373	323.5	2.4	0.7	0.0508	-	-	-	-	(101), (112), (200), (211), (204)	30.5
350	2030	97.8	1.1	1.1	0.0482	-	105.0	3.85	4.0	N.A.	N.A.

[1] Duplicated sample grown at 200 °C.

[2] Sample too rough for XRR measurement.

[3] Duplicated sample grown at 300 °C.

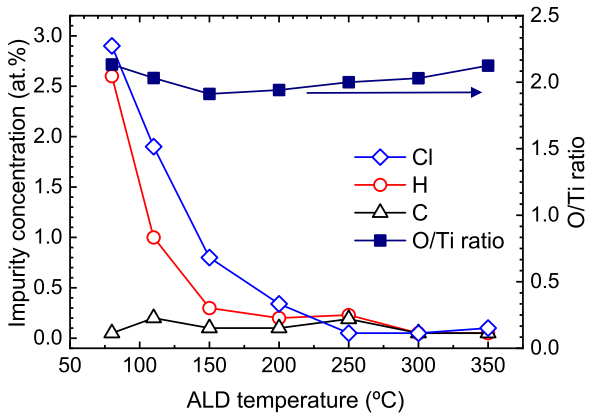

Fig. 2. Impurity concentrations and O/Ti ratio as a function of ALD temperature. Targeted film thickness was 100 nm. Results for the 110, 200 and 300 °C samples were published already in Ref. [48], and for 150 and 250 °C samples in Ref. [54], and repeated here for completeness.

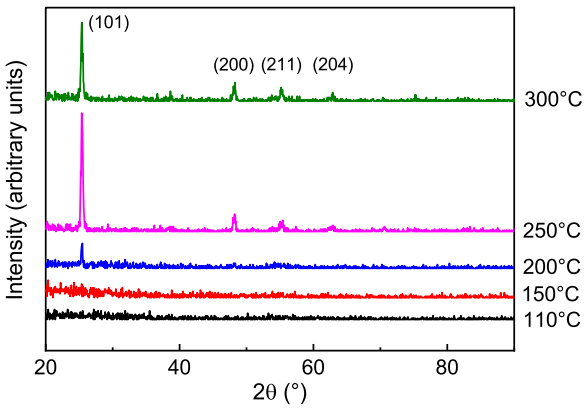

Fig. 3. GIXRD peaks for ALD TiO_2 samples grown at temperatures from 110 to 300 °C. Targeted film thickness for these samples was 100 nm.

factors: the substrate thickness (380 ± 5 μm) of about 5 MPa, the film thickness (100 ± 1 nm) of about 2 MPa, and bow and wafer placement uncertainty for 120 mm scan length causing error in measurement repeatability. Maximum measurement uncertainty thus varies between individual samples.

Besides measuring as-grown films, the influence of the storage time to residual stress was studied by means of wafer curvature measurement with duplicated samples using both Veeco DEKTAK V200-Si and Toho Technology FLX-2320-S tools. With first tool, the first measurement was done within 30 min after ALD process was finished and repeated after one day, two days, one week, and continued with increasing time interval. With the latter tool, the first measurement was made within 30 min after the ALD process was finished and repeated in 5-minutes intervals during 72-hour measurement period. During about 220 days measurement period, the wafers were stored in ISO 4 cleanroom. The Toho Technology FLX-2320-S was also used for analyzing the thermal stability of the as-grown film by thermal cycling. The wafer curvature was measured in-situ during the thermal cycling. The controlled heating rate was 10 °C/min, from 25 to 500 °C, and cooling back to room temperature took more time. This heating-cooling cycle was repeated three times continuously for each sample. During the thermal cycling wafers were under continuous nitrogen flow.

Nanoindentation was performed with a Hysitron Triboindenter for the elastic modulus and hardness using a cube-corner indenter with a 90° total induced angle and 40 nm tip radius. The indent depth was kept less than 10 % of the film thickness. The elastic modulus was determined also with laser-generated surface acoustic wave (LSAW) measurements using the density values measured by XRR. The elastic modulus values were calculated using Poisson's ratio of 0.27 [46] for ALD TiO_2. Measurement methods are described in detail in Ref [52].

3. Results

3.1. Structural and optical properties

Thickness as a function of ALD cycles for TiO_2 films grown at 110, 200 and 300 °C is presented in Fig. 1a. Thickness increase was linear as a function of ALD cycles at 110 °C, except for the thinnest sample (192 cycles), which had substantially lower average growth per cycle (GPC) value compared to the other samples. For films grown at 200 and 300 °C, growth was slightly nonlinear with upward curvature. The growth nonlinearity was largest with TiO_2 grown at 200 °C. In every case, the extrapolated intercept with y-axis was negative, most probably because of the change in growth upon onset of crystallization, as crystallites grow faster than amorphous material.

With increasing ALD temperature, GPC decreased at temperature range from 80 to 200 °C (Table 1 and Fig. 1b). For films grown at higher temperatures, above 200 °C, GPC was higher, and remained nearly constant, independent of the growth temperature. Films grown at 250 °C and up were uniform in thickness, as the st.dev. was ~1% for about 100 nm thick films, compared to the higher non-uniformity of ≥ 2% of the films grown at lower temperatures. The refractive index, measured with ellipsometry, increased from 2.4 to 2.7, as ALD temperature was increased from 110 to 300 °C, except for a drop around 250 °C.

XRR density and roughness increased with increasing ALD temperature, as presented in Table 1. The density was experiencing a similar drop, around 250 °C, as detected for refractive index. With increasing film thickness, from about 10 to 100 nm, XRR roughness increased from 0.4 to 1.2 nm, and 1.0 to 4.3 nm for films grown at 200 and 300 °C, respectively.

According to TOF-ERDA and RBS, the impurity concentration decreased with increasing growth temperature. Impurities and O/Ti ratio for 100 nm TiO_2 are presented in Fig. 2. The main impurity was chlorine and its concentration decreased from 2.9 ± 0.1 to <0.05 at. %, as the ALD temperature was increased from 80 to 350 °C. Hydrogen concentration was at maximum, 2.6 ± 0.2 at. %, at lowest growth temperature, and decreased to under detection limit of < 0.05 at. % at 350 °C. The O/Ti-ratio remained near stoichiometric TiO_2.

The as-grown TiO_2 was amorphous at low growth temperatures, 80, 110 and 150°C, and at lower film thicknesses (Table 1 and Fig. 3). A polycrystalline film with anatase was observed for about 50 nm TiO_2 film, grown at 200°C. For films grown at 300 °C, anatase phase was already detected for about 10 nm film. No other phases were detected. Crystallite size (Table 1) did not change with a systematic manner, as at 200 °C the crystallite size was at largest on thinnest polycrystalline film, thereafter decreased, and again increased with around 380 nm thick film.

The AFM rms surface roughness for about 100 nm TiO_2 samples, grown at 200, 250, 300 and 350 °C, decreased with increasing growth temperature; rms values were 8.5, 6.3, 6.4 and 5.8 nm, respectively. AFM images are presented in Fig. 4. Large plate-like crystals with some large grains were detected for sample grown at 200 °C. For sample grown at 250 °C, grains were larger compared to 200 °C sample, and for samples grown at 300 and 350 °C, the grain size decreased.

ALD TiO_2 films were characterized also after the post-ALD annealing. The film thicknesses, measured by reflectometry, increased slightly due to annealing for samples grown at 110°C (Table 2). With sample grown at 300 °C, a thickness change was detected only after annealing at 900 °C. The hydrogen concentration decreased for sample grown at 110 °C upon annealing. For samples grown at 300 °C, no major changes in impurity content were detected, and most of the values were near or under the detection limit. Density measured by XRR increased upon the

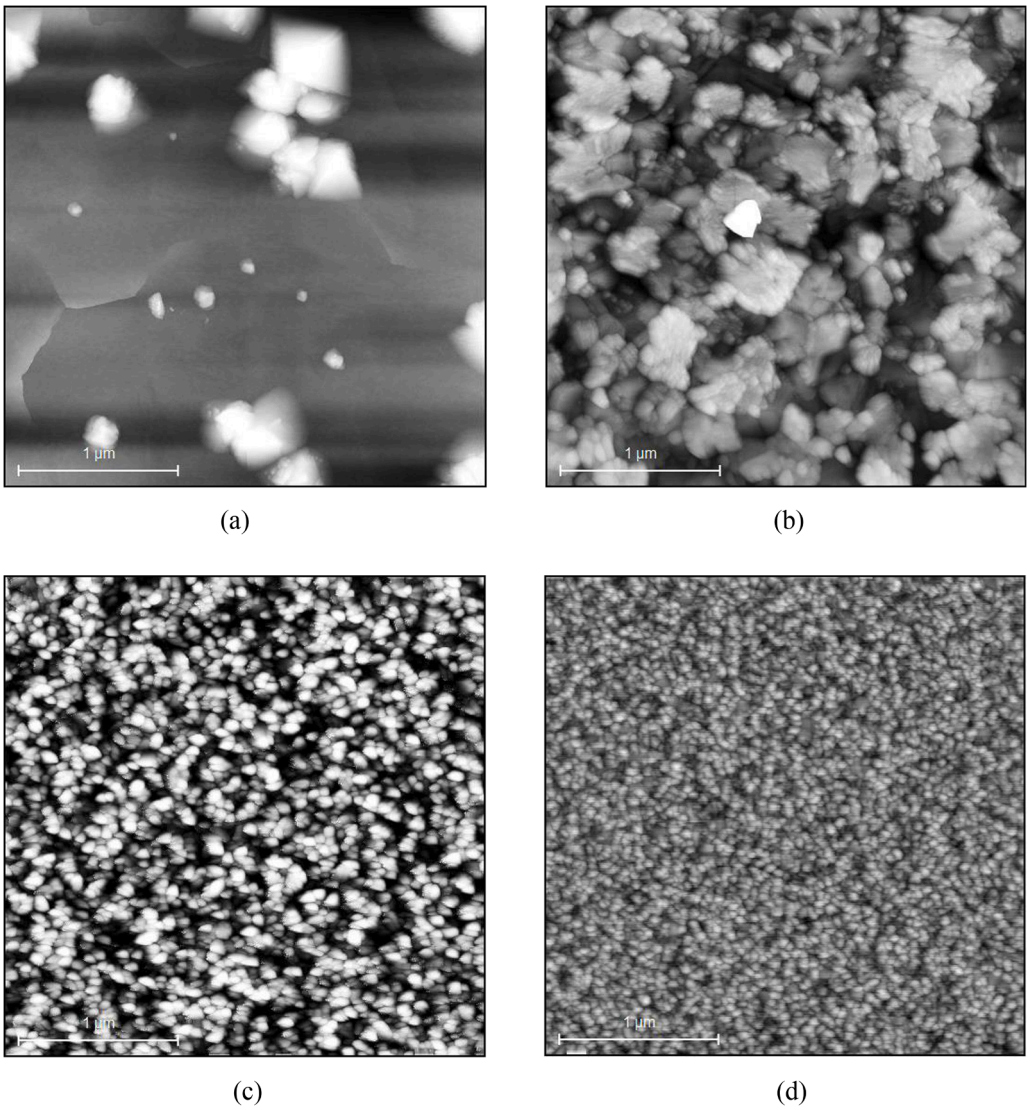

Fig. 4. AFM images of TiO_2 grown at (a) 200 °C, (b) 250 °C, (c) 300 °C, and (d) 350 °C using 2467, 1953, 2124, and 2030 growth cycles, respectively, composed of 0.1-4.0-0.1-4.0 s pulse-purge sequence. Image scale was 3 x 3 µm and sample size 512. In (b) one particle detected in Figure was excluded from analysis (marked with the square).

transition from anatase to rutile (sample grown at 300 °C and annealed at 900 °C), but appeared to decrease with sample grown at 110 °C and annealed at 450 °C.

Refractive index, n and extinction coefficient, k were characterized as a function of the wavelength, from ultraviolet to infrared, from 190 to 1650 nm wavelengths, for as-grown and post-ALD annealed samples. The results are presented in Fig. 5. The sample grown at 110 ºC, had foggy surface after post-ALD annealing at 300 ºC; no measurable change was detected in refractive index or extinction coefficient, the latter remained at a zero value for wavelength range from 380 to 1645 nm. Only after annealing at 450 ºC, a clear drop was seen in refractive index, and in extinction coefficient a change at wavelengths below 380 nm, and again from 1470 nm upwards. Film grown at 200 °C had $k > 0$ throughout the wavelength range. Film grown at 300 °C had a zero k value at wavelength range from 380 to 485 nm, and no change was detected upon annealing at 450 °C. Change in refractive index and k values were seen after post-ALD annealed at 900 ºC.

3.2. Residual stress

The residual stress was measured for samples grown at different temperatures and with different film thicknesses. Fig. 6 presents the residual stress of ALD TiO_2 as a function of film thickness for films grown at 110, 200 and 300 °C. Amorphous films were measured to have about the same level of residual stress, independent of the ALD temperature. For TiO_2 grown at 200 °C, with onset of crystallization, the residual stress first increased with increasing film thickness, reached a maximum for about 100 nm film and thereafter decreased. The residual stress for TiO_2 films grown at 300 °C decreased slightly with increasing film thickness. When the residual stress of about 100 nm samples were studied as a function of the ALD temperature, presented in Table 3, the residual stress reached the maximum level with onset of crystallization around 200 °C, and thereafter decreased.

The residual stress was also characterized as a function of storage time in air after the film growth. The first measurement was done within 30 minutes after the ALD process was finished, and measurements were repeated with increasing time intervals during 220 days measurement period. The residual stress values, based on stylus profilometry results, showed somewhat deviation from measurement to measurement (Fig. 7) and it seemed that there was a continuous decrease in residual stress with sample grown at 300 °C, as the stress relaxed some from 540 to 470 MPa during the storage. The shelf-lifetime series was repeated with a

Table 2
Thin film characterization results of ALD TiO_2 samples grown at 110, 200 and 300 °C after the ALD and post-ALD annealing at 300, 450 and 900 °C are presented here. Measurement uncertainty of the residual stress measurement is in MPa and it presents uncertainty of the measurement system. Wafer curvature measurements were made with Toho Technology FLX-2320-S.

ALD growth					Post-ALD annealing				Thin film characterization																
Temp	Film thickness		Residual stress		Temp	Film thickness		Residual stress		XRR density	XRR roughness	Chemical composition [atm.%]													GIXRD
[°C]	[nm]	st.dev	MPa	±	[°C]	[nm]	st.dev	MPa	±	[g/cm^3]	[nm]	H	±	C	±	Cl	±	O	±	Ti	±		
110	99.2	3.2	413	17	-	-	-	-	-	3.65	0.6	0.80	0.10	<0.05	-	1.50	0.20	66	1	32	1	**	
110	99.8	3.3	413	17	300	101.6	5.7	260	13	3.75	0.8	0.40	0.10	0.15	0.05	1.70	0.20	66	1	32	1	anatase	
110	99.5	3.3	415	17	450	106.7	4.5	128	5	3.45	0.9	0.40	0.10	0.18	0.05	1.90	0.20	65	1	32	1	anatase	
200	103.8	4.6	630	37	-	-	-	-	-	3.75	1.0	0.10	0.05	<0.05	-	0.20	0.10	67	1	33	1	anatase	
300	108.7	1.0	327	13	-	-	-	-	-	3.85	4.5	<0.10	-	<0.10	-	<0.05	-	67	1	33	1	anatase	
300	108.6	1.0	316	12	450	108.7	1.0	348	13	3.85	4.5	<0.10	-	<0.10	-	<0.05	-	67	1	33	1	anatase	
300	108.0	1.3	329	12	900	110.1	0.9	967	26	4.15	4.0	0.20	0.10	0.10	0.05	<0.05	-	68	1	32	1	rutile	

* amorphous film

new sample series and more precise measurement equipment (Toho Technology FLX-2320-S, laser profilometry). Results showed no changes in residual stress upon 220 days measurement period.

Selected samples grown at 110 and 300 °C were annealed after the ALD at 300, 450 and 900 °C. The residual stress was measured before and after the annealing using Toho Technology FLX-2320-S. Due to post-ALD annealing, the residual stress decreased for samples grown at 110 °C, from initial 413 to 260 MPa, and further to 128 MPa, when annealed at 300 and 450 °C, respectively as presented in Table 2. For samples grown at 300 °C, the residual stress increased with increasing post-ALD annealing temperature.

The temperature cycling, made with in-situ wafer curvature measurement using Toho Technology FLX-2320-S tool, from room temperature up to 500 °C and back to room temperature, showed differences in thermal behavior between the samples grown at different temperatures, from 110 to 300 °C, presented in Fig. 8. The residual stress curve of the TiO_2 film grown at 300 ºC was reversible and returned close to its original value, initially starting from 450 MPa and ending to 385 MPa. In films grown at lower temperatures, at 110 and 200 ºC, irreversible change in the residual stress was detected already during the first heat cycle around 440 and 260 °C, respectively, as there was an abrupt rise detected in stress values. In following heating and cooling cycles, no further changes were detected. The sample grown at 110 °C had rise in residual stress from initial 440 to 840 MPa and the sample grown at 200 °C had similar rise in initial residual stress from 470 to 780 MPa.

3.3. Elastic modulus and hardness

Elastic modulus values were measured with two methods: nanoindentation and LSAW, and the values are reported in Table 3 as a function of film thickness and ALD temperature. Approximately stable elastic modulus values were measured with nanoindentation for films grown at temperatures below 300 °C. Films grown at 300 °C and above had somewhat higher elastic modulus values, although with higher result deviation.

The elastic modulus values measured with LSAW for about 100 nm films increased with increasing ALD temperature from about 107 to 170 GPa, as growth temperature was increased from 80 to 200 °C. At higher temperatures, slightly lower modulus values were measured as presented in Table 3. In addition, with increasing film thickness, the maximum modulus was measured from about 70 to 230 nm thick films grown at 200 °C with onset of crystallization. For samples grown at 300 °C, the modulus values decreased from 175 to 165 GPa with increasing film thickness.

Hardness, measured with nanoindentation from about 100 nm thick films, increased from 6.7 to 10.5 GPa with increasing ALD temperature (Table 3), from 80 to 250 °C and thereafter stabilized. Maximum hardness was measured for thinnest sample grown at 300 °C, and at this temperature hardness decreased with increasing film thickness.

4. Discussion

The growth of the ALD TiO_2 was studied as a function of ALD cycles at different temperatures. For amorphous films, grown at 110 °C, linear growth as a function of the ALD cycles was measured. Slight non-linear growth as a function of ALD cycles was detected for films grown at 200 and 300 °C. The non-linear growth behavior, usually accompanied with onset of crystallization [5,61,62], was most noticeable for films grown at 200 °C. Consequently, the thicker the film, the larger was the average GPC, calculated by dividing the measured thickness with ALD cycles. One reason for the origin of the increased GPC could be faster growth of the crystallites in the upward direction, leading to increased surface area, and thus measured thickness [63]. Also increased hydroxyl group (OH) density upon crystallization has been reported to cause increase in the GPC [61,64]; in this work, we can neither confirm nor exclude such an effect.

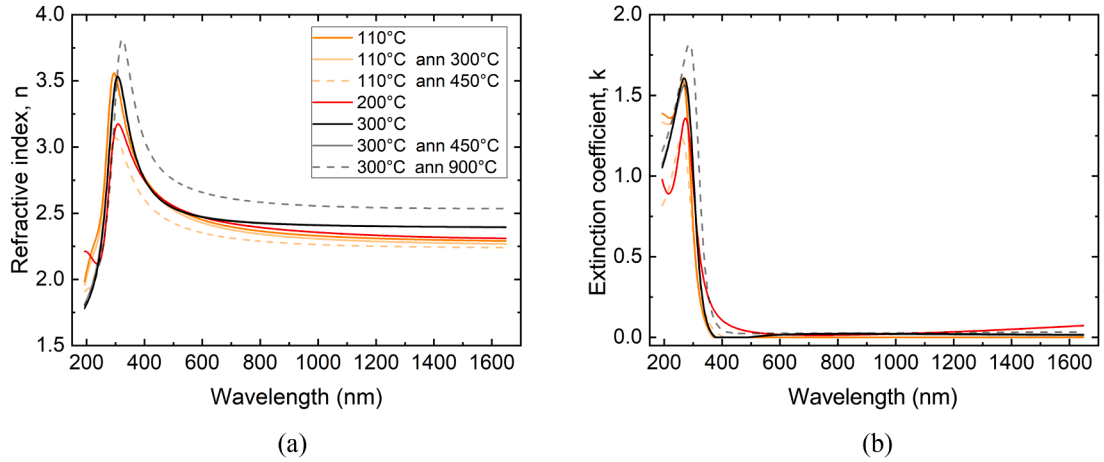

Fig. 5. (a) Refractive index presented as a function of wavelength for samples grown at 110, 200, and 300 °C and for selected samples annealed at 300, 450, and 900 °C. Wavelength range was from 190 to 1645 nm. In (b) the extinction coefficient for the same samples is presented as a function of wavelength.

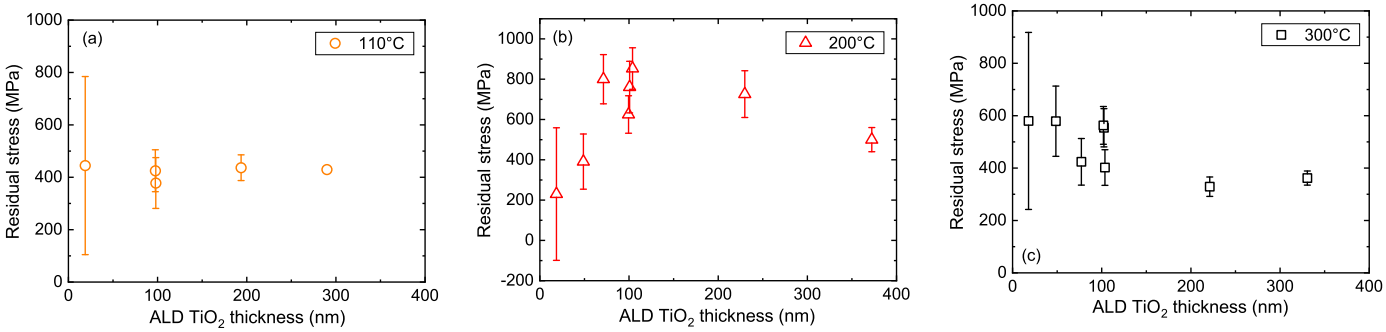

Fig. 6. Residual stress is presented as a function of the film thickness for films grown at (a) 100, (b) 200, and (c) 300 °C. The symbols present median stress values and bars present calculated maximum measurement uncertainty.

Table 3
The residual stress, elastic modulus and hardness as a function of the film thickness and ALD temperature.

ALD temperature	Film thickness	Wafer curvature measurement		Nanoindentation				LSAW	
		Residual stress		Elastic modulus		Hardness		Elastic modulus	
[°C]	[nm]	[MPa]	±	[GPa]	st.dev	[GPa]	st.dev	[GPa]	st.dev
80	97	452*	29	156	19	6.7	0.3	107.4	0.4
110	98	413*	32	152	5	6.9	0.1	126.7	0.5
150	98	382	78	149	4	7.3	0.1	129.0	0.5
200	19	230	329	-	-	-	-	128.0	3.4
	49	391	137	-	-	-	-	137.4	2.9
	71	800	122	-	-	-	-	172.2	0.6
	101	630*	51	154	8	8.5	1.0	171.2	0.6
	230	726	116	-	-	-	-	173.2	0.3
	370	500	60	-	-	-	-	125.6	0.3
250	102	684	77	159	7	10.5	0.8	153.4	0.1
300	23	580	338	165	16	13.6	1.7	175.2	1.1
	48	579	134	170	10	11.2	0.7	166.9	0.4
	102	327*	19	165	16	9.7	1.0	166.5	0.6
	324	362	27	167	45	7.9	2.0	164.4	0.0
350	98	304*	19	165	15	9.6	1.4	167.5	0.6

* Measured with Toho Technology FLX-2320-S.

The optical and structural characterization of these films revealed a drop around 250 °C in refractive index and density, this is in line with previous results [44]. At this temperature, AFM revealed a rough surface, with large grains and platelets. The rough layer characteristics might explain the drop detected in refractive index and density. Refractive index correlated well with the density at ALD temperatures below 250 °C. Both chlorine and hydrogen concentrations decreased with the increasing growth temperature, as reported earlier [28] and there was a negative correlation in the refractive index and chlorine concentration with the increasing growth temperature.

A plot of the extinction coefficient as a function of the wavelength for film grown at 110 °C, showed that film has zero *k* for wavelength range from 380 to 1645 nm, and also after post-ALD annealing at 450 °C, meaning that film is not absorbing at this wavelength range. The film grown at 300 °C, had zero *k* value at wavelength range from 380 to 485 nm, and annealing at higher temperature (900 °C) lead to rise in *k*. Film

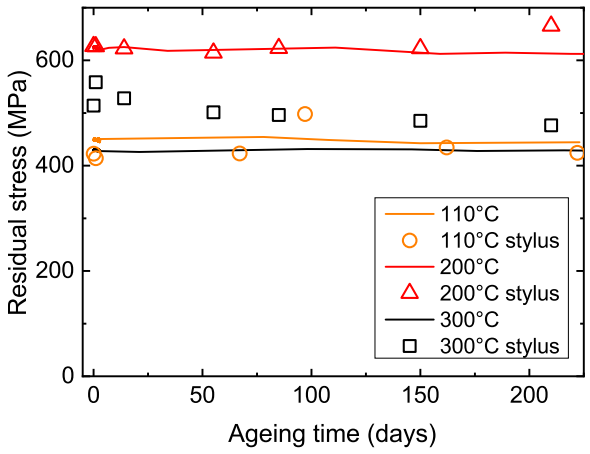

Fig. 7. Residual stress presented as a function of storage time. For samples grown at 110, 200 and 300 °C measured using two different tools.

grown at 200 °C, was absorbing through the wavelength range, though at low levels.

The TiO_2 was detected to be amorphous at low growth temperatures. Anatase peak was detected in GIXRD for about 50 nm films grown at 200 °C. At higher temperature, 300 °C, anatase peaks were already present for 10 nm thick film. These findings correlate with previously published results, but onset of crystallization has been slightly varying depending on the study [23,34–37,65,20]. The grain size correlates with the earlier findings for ALD TiO_2 on silicon [32,65] as for polycrystalline samples, the grain size decreased with increasing ALD temperature.

The change in residual stress of ALD TiO_2 is linked with changes in crystallinity detected by GIXRD and AFM. For the amorphous films, the residual stress was stable as a function of the film thickness, in accordance with findings made for other amorphous ALD materials: Al_2O_3 [52], and Al_2O_3-TiO_2 nanolaminates [54]. At 200 °C, where the onset of crystallization was detected, elevated residual stress was measured. In addition, a large variation in residual stress was detected for duplicated samples grown at 200 °C, and also different anatase peaks were observed in GIXRD. The finding of Lyytinen et al. [48] supports the observation that even between the duplicated samples the crystallization is not progressing in the same stage, as they detected the sample grown at 200 °C (sample included also in this study) to have an mixture of anatase agglomerates in an amorphous matrix. On base of these findings, probably random nucleation of anatase crystallites influence the nucleation phase and order of crystallinity between the duplicated samples as different diffraction peaks were observed in GIXRD (Table 1).

The residual stress measured for TiO_2 in this work is compared with earlier results in Fig. 9. Considering the stress variation detected in this work even for duplicated samples, the results agree well with most numerical results published [44,13,48] for ALD TiO_2 on silicon, and support the conclusion that the residual stress of the ALD TiO_2 is a sensitive function of process parameters. Small fluctuations in temperature, film thickness and precursor doses most likely affect the crystallization and thereby the residual stress.

The effect of post-ALD annealing has been studied on ALD TiO_2 films mainly for structural properties [66] but also for residual stress [13]. For initially amorphous sample grown at 120 °C post-ALD annealing has been reported to increase residual stress [13]. In this work, the residual stress decreased due to film cracking with increasing post-ALD annealing temperatures for samples grown at 110 °C. This is assumed to be caused by the crystallization and related increase in density upon annealing of the initially amorphous film. The film grown at 300 °C and annealed at 900 °C (Table 3), experienced a notable rise in the residual stress after annealing at 900 °C, upon structural change from anatase to rutile. The residual stress remained unchanged during the repeated thermal cycling of sample grown at 300 °C, indicating 500 °C temperature was not high enough to initiate structural changes in the anatase film. The films grown at lower temperatures 110 and 200 °C experienced non-reversible abrupt rise in residual stress already during the first heating cycle at temperatures of 440 and 260 °C, respectively. In this sense results presented here were in line with Jõgi et al.[67] as according to their result the crystallization of the amorphous film to anatase is easier than re-crystallization from anatase to rutile, as large anatase grain size retards the phase transformation, and higher thermal activation energy is needed to initiate rutile nucleation [66,67].

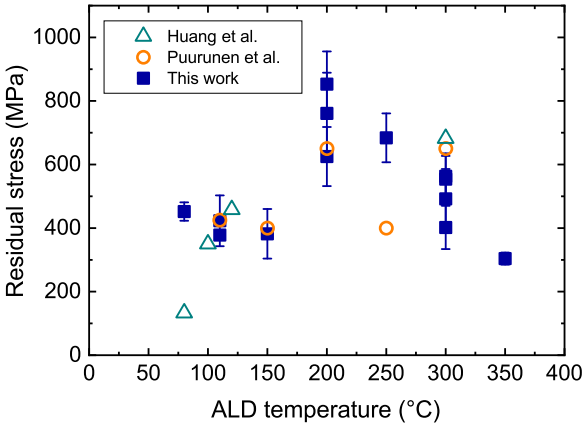

Fig. 9. Comparison of published ALD TiO_2 stress data as a function of ALD temperature. Symbol (■) refers to results presented in this work and is the residual stress value; bars present calculated maximum measurement uncertainty values.

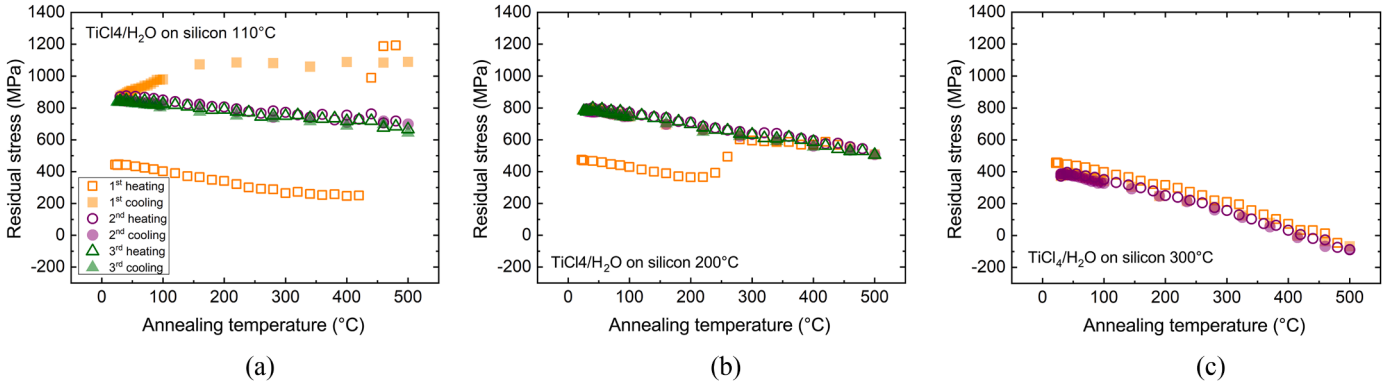

Fig. 8. Residual stress measured in-situ during the repeated post-ALD thermal cycling for films grown at (a) 110 (b) 200 and (c) 300°C. The heating ramp rate was 10 °C/min and temperature range was from about room temperature up to 500 °C and during the subsequent cooling back to about room temperature.

Thickness change during the post-ALD annealing, was most probably due to growth of interfacial SiO_2, proposed already by Methapanon et al. [25] and McDonnell et al.[29]. Hydrogen was the only impurity that was detected to decrease upon thermal annealing; at a general level, Jõgi et al. [67] have reported the post-ALD annealing to decrease impurities and increase amount of crystalline phases.

Change in elastic modulus was mainly attributed to change in crystalline structure, as the highest elastic modulus values were measured around crystallization temperature. The elastic modulus values measured with LSAW showed more temperature, and thickness dependency than the elastic modulus derived from nanoindentation measurements. In principle, the methods should yield the same values for the isotropic films, but systematic differences may emerge as the nanoindentation measurement may suffer from the substrate effect, especially with the crystalline materials. For the LSAW measurement, the surface roughness should not influence to the elastic modulus result, in the roughness range studied in this paper [68].

There are several sources reporting mechanical properties of thin films to have strong correlation with film density [69,70]. In this study, no linear correlation between density and hardness or residual stress was detected, but upon structural transition, changes in stress, elastic modulus and hardness were detected.

5. Conclusions

The purpose of this work was to gain better understanding of mechanical and system properties of ALD TiO_2 and their dependency to the growth temperature and subsequent thermal steps. The structural transition from the amorphous to polycrystalline film upon higher growth temperature caused rise in the tensile residual stress, elastic modulus and hardness of the as-deposited ALD TiO_2. For crystalline films, the post-ALD annealing increased tensile residual stress further, while for amorphous films, the stress decreased slightly upon adhesion failure and loss of film integrity. The optical properties were dependent on film morphology; the onset of crystallization likely caused an increase in scattered light (not necessarily absorbed light) which resulted in an increase of the extinction coefficient, while the amorphous film had zero extinction coefficient on wide wavelength range. Films grown at 110 and 300 °C were able to withstand post-ALD annealing up to 420 °C without major change in residual stress, refractive index or extinction coefficient, which is advantageous considering common post-ALD processing temperatures.

Authors' statement

Oili Ylivaara designed the experiments together with Andreas Langner and Riikka Puurunen. Oili Ylivaara fabricated the samples and made the thickness, AFM and residual stress measurements, and carried out related analysis under supervision of Riikka Puurunen. Andreas Langner made the refractive index and extinction coefficient measurements. Xuwen Liu made the nanoindentation measurements and related data analysis under supervision of Simo-Pekka Hannula. Dieter Schneider made LSAW measurements and related data analysis. Jaakko Julin and Kai Arstila made TOF-ERDA measurements and related data analysis under supervision of Timo Sajavaara. Sakari Sintonen and Saima Ali made the XRR and GIXRD measurements and the data analysis under supervision of Harri Lipsanen. Project administration, supervision and resource management was done by Riikka Puurunen. Different measurements were done by persons mentioned in author statement. In addition Oili Ylivaara did writing of the original draft and also writing and editing of the review. All authors discussed the results and commented the manuscript by Oili Ylivaara.

Declaration of Competing Interest

None

Acknowledgment

This work was carried out within the MECHALD project funded by Business Finland (Tekes) and is linked to the Finnish Centers of Excellence in Atomic Layer Deposition (ref. 251220) and Nuclear and Accelerator Based Physics (refs. 213503 and 251353) of the Academy of Finland.

References

[1] U. Diebold, The surface science of titanium dioxide, Surf. Sci. Rep. 48 (2003) 53–229, https://doi.org/10.1016/S0167-5729(02)00100-0.
[2] F. De Angelis, C. Di Valentin, S. Fantacci, A. Vittadini, A. Selloni, Theoretical studies on anatase and less common TiO_2 phases: bulk, surfaces, and nanomaterials, Chem. Rev. 114 (2014) 9708–9753, https://doi.org/10.1021/cr500055q.
[3] M. Ritala, M. Leskelä, E. Nykänen, P. Soininen, L. Niinistö, Growth of titanium dioxide thin films by atomic layer epitaxy, Thin Solid Films 225 (1993) 288–295, https://doi.org/10.1016/0040-6090(93)90172-L.
[4] J. Aarik, A. Aidla, T. Uustare, V. Sammelselg, Morphology and structure of TiO_2 thin films grown by atomic layer deposition, J. Cryst. Growth 148 (1995) 268–275, https://doi.org/10.1016/0022-0248(94)00874-4.
[5] V. Miikkulainen, M. Leskelä, M. Ritala, R.L. Puurunen, Crystallinity of inorganic films grown by atomic layer deposition: overview and general trends, J. Appl. Phys. 113 (2013), 021301, https://doi.org/10.1063/1.4757907.
[6] J.-P. Niemelä, G. Marin, M. Karppinen, Titanium dioxide thin films by atomic layer deposition: a review, Semicond. Sci. Technol. 32 (2017), 093005, https://doi.org/10.1088/1361-6641/aa78ce.
[7] S. Won, S. Go, W. Lee, K. Jeong, H. Jung, C. Lee, E. Lee, J. Lee, Effects of defects generated in ALD TiO_2 films on electrical properties and interfacial reaction in TiO2/SiO2/Si system upon annealing in vacuum, Met. Mater. Int. 14 (2008) 759–765, https://doi.org/10.1007/BF03027993.
[8] T. Nabatame, A. Ohi, T. Chikyo, M. Kimura, H. Yamada, T. Ohishi, Electrical properties of anatase TiO_2 films by atomic layer deposition and low annealing temperature, J. Vac. Sci. Technol. B Nanotechnol. Microelectron. Mater. Process. Meas. Phenom. 32 (2014) 03D121, https://doi.org/10.1116/1.4869059.
[9] C. Das, K. Henkel, M. Tallarida, D. Schmeißer, H. Gargouri, I. Kärkkänen, J. Schneidewind, B. Gruska, M. Arens, Thermal and plasma enhanced atomic layer deposition of TiO_2 : comparison of spectroscopic and electric properties, J. Vac. Sci. Technol. A 33 (2015) 01A144, https://doi.org/10.1116/1.4903938.
[10] J. Aarik, A. Aidla, A.-A. Kiisler, T. Uustare, V. Sammelselg, Effect of crystal structure on optical properties of TiO_2 films grown by atomic layer deposition, Thin Solid Films 305 (1997) 270–273, https://doi.org/10.1016/S0040-6090(97)00135-1.
[11] Y.-Q. Hou, D.-M. Zhuang, G. Zhang, M. Zhao, M.-S. Wu, Influence of annealing temperature on the properties of titanium oxide thin film, Appl. Surf. Sci. 218 (2003) 98–106, https://doi.org/10.1016/S0169-4332(03)00569-5.
[12] A. Szeghalmi, M. Helgert, R. Brunner, F. Heyroth, U. Gösele, M. Knez, Atomic layer deposition of Al_2O_3 and TiO_2 multilayers for applications as bandpass filters and antireflection coatings, Appl. Opt. 48 (2009) 1727–1732, https://doi.org/10.1364/AO.48.001727.
[13] Y. Huang, G. Pandraud, P.M. Sarro, Characterization of low temperature deposited atomic layer deposition TiO_2 for MEMS applications, J. Vac. Sci. Technol. A 31 (2013) 01A148, https://doi.org/10.1116/1.4772664.
[14] D. Saha, R.S. Ajimsha, K. Rajiv, C. Mukherjee, M. Gupta, P. Misra, L.M. Kukreja, Spectroscopic ellipsometry characterization of amorphous and crystalline TiO2 thin films grown by atomic layer deposition at different temperatures, Appl. Surf. Sci. 315 (2014) 116–123, https://doi.org/10.1016/j.apsusc.2014.07.098.
[15] G.S. Sveshnikova, S.I. Kol'tsov, V.B. Aleskovskii, Interaction of titanium tetrachloride with hydroxylated silicon surfaces, J. Appl. Chem. USSR 43 (1970) 432–434.
[16] R.L. Puurunen, A Short history of atomic layer deposition: Tuomo Suntola's atomic layer epitaxy, Chem. Vap. Depos. 20 (2014) 332–344, https://doi.org/10.1002/cvde.201402012.
[17] A.A. Malygin, V.E. Drozd, A.A. Malkov, V.M. Smirnov, From V. B. Aleskovskii's "Framework" hypothesis to the method of molecular layering/atomic layer deposition, Chem. Vap. Depos. 21 (2015) 216–240, https://doi.org/10.1002/cvde.201502013.
[18] E. Ahvenniemi, A.R. Akbashev, S. Ali, M. Bechelany, M. Berdova, S. Boyadjiev, D. C. Cameron, R. Chen, M. Chubarov, V. Cremers, A. Devi, V. Drozd, L. Elnikova, G. Gottardi, K. Grigoras, D.M. Hausmann, C.S. Hwang, S.-H. Jen, T. Kallio, J. Kanervo, I. Khmelnitskiy, D.H. Kim, L. Klibanov, Y. Koshtyal, A.O.I. Krause, J. Kuhs, I. Kärkkänen, M.-L. Kääriäinen, T. Kääriäinen, L. Lamagna, A.A. Łapicki, M. Leskelä, H. Lipsanen, J. Lyytinen, A. Malkov, A. Malygin, A. Mennad, C. Militzer, J. Molarius, M. Norek, Ç. Özgit-Akgün, M. Panov, H. Pedersen, F. Piallat, G. Popov, R.L. Puurunen, G. Rampelberg, R.H.A. Ras, E. Rauwel, F. Roozeboom, T. Sajavaara, H. Salami, H. Savin, N. Schneider, T.E. Seidel, J. Sundqvist, D.B. Suyatin, T. Törndahl, J.R. van Ommen, C. Wiemer, O.M. E. Ylivaara, O. Yurkevich, Review Article: Recommended reading list of early publications on atomic layer deposition—outcome of the "Virtual Project on the History of ALD", J. Vac. Sci. Technol. A 35 (2017) 010801, https://doi.org/10.1116/1.4971389, 010801.

[19] J. Aarik, A. Aidla, V. Sammelselg, H. Siimon, T. Uustare, Control of thin film structure by reactant pressure in atomic layer deposition of TiO_2, J. Cryst. Growth. 169 (1996) 496–502, https://doi.org/10.1016/S0022-0248(96)00423-X.

[20] V. Sammelselg, A. Rosental, A. Tarre, L. Niinistö, K. Heiskanen, K. Ilmonen, L.-S. Johansson, T. Uustare, TiO_2 thin films by atomic layer deposition: a case of uneven growth at low temperature, Appl. Surf. Sci. 134 (1998) 78–86, https://doi.org/10.1016/S0169-4332(98)00224-4.

[21] J. Aarik, A. Aidla, H. Mändar, V. Sammelselg, Anomalous effect of temperature on atomic layer deposition of titanium dioxide, J. Cryst. Growth 220 (2000) 531–537, https://doi.org/10.1016/S0022-0248(00)00897-6.

[22] J. Aarik, A. Aidla, H. Mändar, T. Uustare, Atomic layer deposition of titanium dioxide from $TiCl_4$ and H_2O: investigation of growth mechanism, Appl. Surf. Sci. 172 (2001) 148–158, https://doi.org/10.1016/S0169-4332(00)00842-4.

[23] K.S. Finnie, G. Triani, K.T. Short, D.R.G. Mitchell, D.J. Attard, J.R. Bartlett, C. J. Barbé, Influence of Si(100) surface pretreatment on the morphology of TiO_2 films grown by atomic layer deposition, Thin Solid Films 440 (2003) 109–116, https://doi.org/10.1016/S0040-6090(03)00818-6.

[24] R.L. Puurunen, Formation of metal oxide particles in atomic layer deposition during the chemisorption of metal chlorides: a review, Chem. Vap. Depos. 11 (2005) 79–90, https://doi.org/10.1002/cvde.200400021.

[25] R. Methaapanon, S.F. Bent, Comparative study of titanium dioxide atomic layer deposition on silicon dioxide and hydrogen-terminated silicon, J. Phys. Chem. C 114 (2010) 10498–10504, https://doi.org/10.1021/jp1013303.

[26] G. Triani, J.A. Campbell, P.J. Evans, J. Davis, B.A. Latella, R.P. Burford, Low temperature atomic layer deposition of titania thin films, Thin Solid Films 518 (2010) 3182–3189, https://doi.org/10.1016/j.tsf.2009.09.010.

[27] J. Dendooven, S. Pulinthanathu Sree, K. De Keyser, D. Deduytsche, J.A. Martens, K. F. Ludwig, C. Detavernier, In situ X-ray fluorescence measurements during atomic layer deposition: nucleation and growth of TiO_2 on planar substrates and in nanoporous films, J. Phys. Chem. C. 115 (2011) 6605–6610, https://doi.org/10.1021/jp111314b.

[28] S.Y. Lee, C. Jeon, S.H. Kim, Y. Kim, W. Jung, K.-S. An, C.-Y. Park, In-situ X-ray photoemission spectroscopy study of atomic layer deposition of TiO_2 on silicon substrate, Jpn. J. Appl. Phys. 51 (2012), 031102, https://doi.org/10.1143/JJAP.51.031102.

[29] S. McDonnell, R.C. Longo, O. Seitz, J.B. Ballard, G. Mordi, D. Dick, J.H.G. Owen, J. N. Randall, J. Kim, Y.J. Chabal, K. Cho, R.M. Wallace, Controlling the atomic layer deposition of titanium dioxide on silicon: dependence on surface termination, J. Phys. Chem. C 117 (2013) 20250–20259, https://doi.org/10.1021/jp4060022.

[30] I. Iatsunskyi, M. Jancelewicz, G. Nowaczyk, M. Kempiński, B. Peplińska, M. Jarek, K. Załęski, S. Jurga, V. Smyntyna, Atomic layer deposition TiO_2 coated porous silicon surface: Structural characterization and morphological features, Thin Solid Films 589 (2015) 303–308, https://doi.org/10.1016/j.tsf.2015.05.056.

[31] I. Kavre Piltaver, R. Peter, I. Šarić, K. Salamon, I. Jelovica Badovinac, K. Koshmak, S. Nannarone, I. Delač Marion, M. Petravić, Controlling the grain size of polycrystalline TiO_2 films grown by atomic layer deposition, Appl. Surf. Sci. 419 (2017) 564–572, https://doi.org/10.1016/j.apsusc.2017.04.146.

[32] D.R.G. Mitchell, D.J. Attard, G. Triani, Transmission electron microscopy studies of atomic layer deposition TiO_2 films grown on silicon, Thin Solid Films 441 (2003) 85–95, https://doi.org/10.1016/S0040-6090(03)00877-0.

[33] D.R.G. Mitchell, G. Triani, D.J. Attard, K.S. Finnie, P.J. Evans, C.J. Barbé, J. R. Bartlett, Atomic layer deposition of TiO_2 and Al_2O_3 thin films and nanolaminates, Smart Mater. Struct. 15 (2006), https://doi.org/10.1088/0964-1726/15/1/010. S57–S64.

[34] A. Niilisk, M. Moppel, M. Pärs, I. Sildos, T. Jantson, T. Avarmaa, R. Jaaniso, J. Aarik, Structural study of TiO_2 thin films by micro-Raman spectroscopy, Open Phys. 4 (2006) 105–116, https://doi.org/10.1007/s11534-005-0009-3.

[35] H.-E. Cheng, C.-C. Chen, Morphological and Photoelectrochemical Properties of ALD TiO_2 Films, J. Electrochem. Soc. 155 (2008) D604, https://doi.org/10.1149/1.2952659.

[36] D.R.G. Mitchell, G. Triani, Z. Zhang, Hydrothermal crystallization of amorphous titania films deposited using low temperature atomic layer deposition, Thin Solid Films 516 (2008) 8414–8423, https://doi.org/10.1016/j.tsf.2008.04.052.

[37] R.L. Puurunen, T. Sajavaara, E. Santala, V. Miikkulainen, T. Saukkonen, M. Laitinen, M. Leskelä, Controlling the crystallinity and roughness of atomic layer deposited titanium dioxide films, J. Nanosci. Nanotechnol. 11 (2011) 8101–8107, https://doi.org/10.1166/jnn.2011.5060.

[38] M.D. McDaniel, A. Posadas, T. Wang, A.A. Demkov, J.G. Ekerdt, Growth and characterization of epitaxial anatase TiO_2(001) on $SrTiO_3$-buffered Si(001) using atomic layer deposition, Thin Solid Films 520 (2012) 6525–6530, https://doi.org/10.1016/j.tsf.2012.06.061.

[39] Q. Tao, K. Overhage, G. Jursich, C. Takoudis, On the initial growth of atomic layer deposited TiO2 films on silicon and copper surfaces, Thin Solid Films 520 (2012) 6752–6756, https://doi.org/10.1016/j.tsf.2012.07.004.

[40] D.C. Cameron, R. Krumpolec, T.V. Ivanova, T. Homola, M. Černák, Nucleation and initial growth of atomic layer deposited titanium oxide determined by spectroscopic ellipsometry and the effect of pretreatment by surface barrier discharge, Appl. Surf. Sci. 345 (2015) 216–222, https://doi.org/10.1016/j.apsusc.2015.03.135.

[41] W. Chiappim, G.E. Testoni, R.S. Moraes, R.S. Pessoa, J.C. Sagás, F.D. Origo, L. Vieira, H.S. Maciel, Structural, morphological, and optical properties of TiO_2 thin films grown by atomic layer deposition on fluorine doped tin oxide conductive glass, Vacuum 123 (2016) 91–102, https://doi.org/10.1016/j.vacuum.2015.10.019.

[42] O.M. Ishchenko, G. Lamblin, D. Arl, N. Adjeroud, J. Guillot, P. Grysan, P. Nukala, J. Guyon, I. Fechete, F. Garin, P. Turek, D. Lenoble, Highly reactive TiO_2 anatase single crystal domains grown by atomic layer deposition, Cryst. Growth Des. 18 (2018) 4929–4936, https://doi.org/10.1021/acs.cgd.8b00170.

[43] L. Borgese, E. Bontempi, M. Gelfi, L.E. Depero, P. Goudeau, G. Geandier, D. Thiaudière, Microstructure and elastic properties of atomic layer deposited TiO_2 anatase thin films, Acta Mater. 59 (2011) 2891–2900, https://doi.org/10.1016/j.actamat.2011.01.032.

[44] R.L. Puurunen, J. Saarilahti, H. Kattelus, Implementing ALD layers in MEMS processing, ECS Trans. 11 (2019) 3–14, https://doi.org/10.1149/1.2779063.

[45] E. Bontempi, P. Zanola, M. Gelfi, M. Zucca, L.E. Depero, B. Girault, P. Goudeau, G. Geandier, E.L. Bourhis, P.-O. Renault, Elastic behaviour of titanium dioxide films on polyimide substrates studied by in situ tensile testing in a X-ray diffractometer, Nucl. Instrum. Methods Phys. Res. Sect. B Beam Interact. Mater. Atoms 268 (2010) 365–369, https://doi.org/10.1016/j.nimb.2009.09.034.

[46] L. Borgese, M. Gelfi, E. Bontempi, P. Goudeau, G. Geandier, D. Thiaudière, L. E. Depero, Young modulus and Poisson ratio measurements of TiO_2 thin films deposited with atomic layer deposition, Surf. Coat. Technol. 206 (2012) 2459–2463, https://doi.org/10.1016/j.surfcoat.2011.10.050.

[47] J. Lyytinen, M. Berdova, P. Hirvonen, X.W. Liu, S. Franssila, Q. Zhou, J. Koskinen, Interfacial mechanical testing of atomic layer deposited TiO_2 and Al_2O_3 on a silicon substrate by the use of embedded SiO_2 microspheres, RSC Adv. 4 (2014) 37320–37328, https://doi.org/10.1039/C4RA05807K.

[48] J. Lyytinen, X. Liu, O.M.E. Ylivaara, S. Sintonen, A. Iyer, S. Ali, J. Julin, H. Lipsanen, T. Sajavaara, R.L. Puurunen, J. Koskinen, Nanotribological, nanomechanical and interfacial characterization of atomic layer deposited TiO_2 on a silicon substrate, Wear 342–343 (2015) 270–278, https://doi.org/10.1016/j.wear.2015.09.001.

[49] L. Kilpi, O.M.E. Ylivaara, A. Vaajoki, X. Liu, V. Rontu, S. Sintonen, E. Haimi, J. Malm, M. Bosund, M. Tuominen, T. Sajavaara, H. Lipsanen, S.-P. Hannula, R. L. Puurunen, H. Ronkainen, Tribological properties of thin films made by atomic layer deposition sliding against silicon, J. Vac. Sci. Technol. A 36 (2018) 01A122, https://doi.org/10.1116/1.5003729.

[50] Y.S. Mohammed, K. Zhang, P. Lin, H. Baumgart, A.A. Elmustafa, Investigation of the nanomechanical properties of crystalline anatase titanium dioxide films synthesized using atomic layer deposition, JOM (2020), https://doi.org/10.1007/s11837-020-04347-6.

[51] V.K. Khanna, Adhesion–delamination phenomena at the surfaces and interfaces in microelectronics and MEMS structures and packaged devices, J. Phys. D. Appl. Phys. 44 (2011), 034004, https://doi.org/10.1088/0022-3727/44/3/034004.

[52] O.M.E. Ylivaara, X. Liu, L. Kilpi, J. Lyytinen, D. Schneider, M. Laitinen, J. Julin, S. Ali, S. Sintonen, M. Berdova, E. Haimi, T. Sajavaara, H. Ronkainen, H. Lipsanen, J. Koskinen, S.-P. Hannula, R.L. Puurunen, Aluminum oxide from trimethylaluminum and water by atomic layer deposition: the temperature dependence of residual stress, elastic modulus, hardness and adhesion, Thin Solid Films 552 (2014) 124–135, https://doi.org/10.1016/j.tsf.2013.11.112.

[53] L. Kilpi, O.M.E. Ylivaara, A. Vaajoki, J. Malm, S. Sintonen, M. Tuominen, R.L.R. L. Puurunen, H. Ronkainen, Microscratch testing method for systematic evaluation of the adhesion of atomic layer deposited thin films on silicon, J. Vac. Sci. Technol. A 34 (2016) 01A124, https://doi.org/10.1116/1.4935959.

[54] O.M.E. Ylivaara, L. Kilpi, X. Liu, S. Sintonen, S. Ali, M. Laitinen, J. Julin, E. Haimi, T. Sajavaara, H. Lipsanen, S.-P. Hannula, H. Ronkainen, R.L. Puurunen, Aluminum oxide/titanium dioxide nanolaminates grown by atomic layer deposition: growth and mechanical properties, J. Vac. Sci. Technol. A 35 (2017) 01B105, https://doi.org/10.1116/1.4966198.

[55] S. Sintonen, S. Ali, O.M.E. Ylivaara, R.L. Puurunen, H. Lipsanen, X-ray reflectivity characterization of atomic layer deposition $Al2O_3/TiO_2$ nanolaminates with ultrathin bilayers, J. Vac. Sci. Technol. A 32 (2014) 01A111, https://doi.org/10.1116/1.4833556.

[56] S. Ali, T. Juntunen, S. Sintonen, O.M.E. Ylivaara, R.L. Puurunen, H. Lipsanen, I. Tittonen, S.-P. Hannula, Thermal conductivity of amorphous $Al2O_3/TiO_2$ nanolaminates deposited by atomic layer deposition, Nanotechnology 27 (2016), 445704, https://doi.org/10.1088/0957-4484/27/44/445704.

[57] U. Holzwarth, N. Gibson, The Scherrer equation versus the 'Debye – Scherrer equation', Nat. Nanotechnol. 6 (2011) 534, https://doi.org/10.1038/nnano.2011.145.

[58] M. Laitinen, T. Sajavaara, M. Rossi, J. Julin, R.L. Puurunen, T. Suni, T. Ishida, H. Fujita, K. Arstila, B. Brijs, H.J. Whitlow, Depth profiling of Al_2O_3+TiO_2 nanolaminates by means of a time-of-flight energy spectrometer, Nucl. Instrum. Methods Phys. Res. Sect. B Beam Interact. Mater. Atoms 269 (2011) 3021–3024, https://doi.org/10.1016/j.nimb.2011.04.074.

[59] G.G. Stoney, The tension of metallic films deposited by electrolysis, Proc. R. Soc. Lond. A 82 (1909) 172–175, https://doi.org/10.1098/rspa.1909.0021.

[60] S. Timoshenko, Analysis of Bi-Metal Thermostats, J. Opt. Soc. Am. 11 (1925) 233–255.

[61] S.K. Kim, S. Hoffmann-Eifert, M. Reiners, R. Waser, Relation between enhancement in growth and thickness-dependent crystallization in ALD TiO_2 thin films, J. Electrochem. Soc. 158 (2011) D6, https://doi.org/10.1149/1.3507258.

[62] E. Langereis, S.B.S. Heil, H.C.M. Knoops, W. Keuning, M.C.M. van de Sanden, W.M. M. Kessels, In situ spectroscopic ellipsometry as a versatile tool for studying atomic layer deposition, J. Phys. D. Appl. Phys. 42 (2009), 073001, https://doi.org/10.1088/0022-3727/42/7/073001.

[63] D.M. Hausmann, R.G. Gordon, Surface morphology and crystallinity control in the atomic layer deposition (ALD) of hafnium and zirconium oxide thin films, J. Cryst. Growth 249 (2003) 251–261, https://doi.org/10.1016/S0022-0248(02)02133-4.

[64] C. Guerra-Nuñez, Y. Zhang, M. Li, V. Chawla, R. Erni, J. Michler, H.G. Park, I. Utke, Morphology and crystallinity control of ultrathin TiO_2 layers deposited on carbon

nanotubes by temperature-step atomic layer deposition, Nanoscale 7 (2015) 10622–10633, https://doi.org/10.1039/C5NR02106E.
[65] W.-J. Lee, M.-H. Hon, Space-limited crystal growth mechanism of TiO2 films by atomic layer deposition, J. Phys. Chem. C 114 (2010) 6917–6921, https://doi.org/10.1021/jp911210q.
[66] J. Lee, S.J. Lee, W.B. Han, H. Jeon, J. Park, W. Jang, C.S. Yoon, H. Jeon, Deposition temperature dependence of titanium oxide thin films grown by remote-plasma atomic layer deposition, Phys. Status Solidi 210 (2013) 276–284, https://doi.org/10.1002/pssa.201228671.
[67] I. Jõgi, M. Pärs, J. Aarik, A. Aidla, M. Laan, J. Sundqvist, L. Oberbeck, J. Heitmann, K. Kukli, Conformity and structure of titanium oxide films grown by atomic layer deposition on silicon substrates, Thin Solid Films 516 (2008) 4855–4862, https://doi.org/10.1016/j.tsf.2007.09.008.
[68] D. Paehler, D. Schneider, M. Herben, Nondestructive characterization of sub-surface damage in rotational ground silicon wafers by laser acoustics, Microelectron. Eng. 84 (2007) 340–354, https://doi.org/10.1016/j.mee.2006.11.001.
[69] O. Anderson, C.R. Ottermann, R. Kuschnereit, P. Hess, K. Bange, Density and Young's modulus of thin TiO_2 films, Fresenius. J. Anal. Chem. 358 (1997) 315–318, https://doi.org/10.1007/s002160050416.
[70] A. Bendavid, P.J. Martin, H. Takikawa, Deposition and modification of titanium dioxide thin films by filtered arc deposition, Thin Solid Films 360 (2000) 241–249, https://doi.org/10.1016/S0040-6090(99)00937-2.